JCTC Journal of Chemical Theory and Computation

Article

pubs.acs.org/JCTC

# Electronic Excitations in Solution: The Interplay between State Specific Approaches and a Time-Dependent Density Functional Theory Description

Ciro A. Guido,[*,†] Denis Jacquemin,[‡,§] Carlo Adamo,[§,∥] and Benedetta Mennucci[*,†]

[†]Dipartimento di Chimica e Chimica Industriale, Università di Pisa, Via Moruzzi 13, 56124 Pisa, Italy

[‡]Laboratoire CEISAM - UMR CNRS 6230, Université de Nantes, 2 Rue de la Houssinière, BP 92208, 44322 Nantes Cedex 3, France

[§]Institut Universitaire de France, 103, bd. Saint-Michel, F-75005 Paris Cedex 05, France

[∥]Institut de Recherche Chimie Paris, PSL University Chimie ParisTech CNRS, 11 rue P. et M. Curie, F-75005 Paris, France

Supporting Information

**ABSTRACT:** We critically analyze the performances of continuum solvation models when coupled to time-dependent density functional theory (TD-DFT) to predict solvent effects on both absorption and emission energies of chromophores in solution. Different polarization schemes of the polarizable continuum model (PCM), such as linear response (LR) and three different state specific (SS) approaches, are considered and compared. We show the necessity of introducing a SS model in cases where large electron density rearrangements are involved in the excitations, such as charge-transfer transitions in both twisted and quadrupolar compounds, and underline the very delicate interplay between the selected polarization method and the chosen exchange-correlation functional. This interplay originates in the different descriptions of the transition and ground/excited state multipolar moments by the different functionals. As a result, the choice of both the DFT functional and the solvent polarization scheme has to be consistent with the nature of the studied electronic excitation.

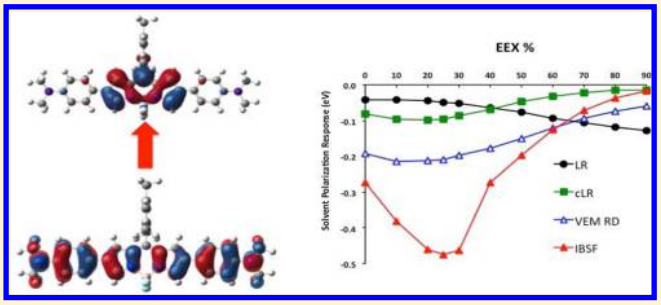


## 1. INTRODUCTION

The absorption and emission processes, together with the geometrical relaxation accompanying the evolution of the excited states, are essential steps for an accurate description of the photophysics and photochemistry of molecular systems. Any time a solvent is present, both absorption and emission processes can be affected together with the corresponding spectroscopic signals such as the position, the intensity, and the shape of the bands.[1,2] These effects are generally referred to as solvatochromism,[2−4] and they are the result of a network of different solute−solvent interactions.[5] The main interactions are generally of electrostatic origin, and they correlate with the solvent polarity. The importance of correctly accounting for the electrostatic effects explains the widespread use of averaged pictures to model the solute−solvent interactions, such as the continuum models[6−8] which have been largely used to describe photochemical and photophysical processes of solvated molecules.[9−16] In particular, formulations based on the time-dependent density functional theory[17] (TD-DFT) in a random phase approximation (RPA) framework[18] opened the way to an impressive number of studies of excited state processes and properties of molecular systems of chemical, biological, and technological interest. However, if the accuracy of TD-DFT results largely depends on the choice of the exchange-correlation (xc) functional,[19] a further source of error can be due to the polarization scheme used to include the solvent effects within continuum models.[6,11] In this study, different polarization schemes of the polarizable continuum model (PCM), derived either from the response theory (generally indicated as linear response, LR)[20−24] or from state specific (SS)[25−29] formulations are critically analyzed, in conjunction with the nature of the xc functional, to describe solvatochromic shifts for both absorption and fluorescence of different types of excited states. The fundamental role of SS corrections is illustrated and analyzed in those cases where large density rearrangements between the ground and excited states exist, e.g., charge-transfer excitations in both twisted or quadrupolar systems. The possibility of error cancellation for CT states computed at the LR-PCM level[30−32] with a global hybrid functional containing a small percentage (less than 30%) of exact exchange is also discussed.

## 2. POLARIZATION SCHEMES FOR CONTINUUM SOLVATION MODELS

In QM/continuum models, once the ground state problem is solved, the solvent and the ground state solute polarization are mutually equilibrated. This equilibrium can be perturbed if the

Received: July 16, 2015
Published: October 27, 2015





DOI: 10.1021/acs.jctc.5b00679
J. Chem. Theory Comput. 2015, 11, 5782−5790

solute charge distribution is rapidly changed, as during "vertical" transition processes. The differences in the characteristic response times of the various degrees of freedom of the solvent may lead to a solvation regime in which the slow components are no longer equilibrated with the excited solute: the resulting regime is usually referred to as "nonequilibrium" solvation, that next slowly evolves into a new equilibrium where all solvent degrees of freedom, including the slow ones, have been relaxed with the new electronic state of the solute. Especially for highly polar solvents, "equilibrium" and "nonequilibrium" solvation regimes represent very different solvent configurations, and the energy difference between the two regimes is generally referred to as the "solvent reorganization energy". The "nonequilibrium" solvation can be properly described within the continuum framework:[33] a simplified but effective formulation is introduced by partitioning the solvent polarization into a dynamic component, mimicking the polarization of the electronic charge of the solvent molecules, and an inertial component collecting all the other contributions (nuclear, molecular).

However, the coupling of the solute QM description with continuum models when describing the environment response following a vertical excitation is neither univocal nor straightforward. During the past decade, two principal formulations have been proposed and tested. The difference between the two approaches can be clarified by reformulating the excitation in solution as a two-step process: in the first step, the molecule in its ground state in equilibrium with the solvent is excited to the $i$th state in the presence of a solvent polarization frozen in the initial ground state; let us call $\omega_{0i}^{0}$ the resulting excitation energy. In the second step, the dynamic component of the solvent polarization rearranges to equilibrate with the excited state charge density of the solute. The excitation energy therefore changes, and one can adopt two different expressions corresponding to a LR or an SS model. Based on a Rayleigh−Schrödinger perturbation theory, Cammi et al.[25] derived comparable expressions for both frameworks, namely:

$$\omega_{0i}^{LR} = \omega_{0i}^{0} + \langle i^{(0)}|\hat{\boldsymbol{V}}|0\rangle\langle 0|\hat{\boldsymbol{Q}}_{\boldsymbol{dyn}}|i^{(0)}\rangle = \omega_{0i}^{0} + R_{dyn}^{LR}(P_{0i}^{T}) \tag{1}$$

$$\omega_{0i}^{SS} = \omega_{0i}^{0} + \frac{1}{2}[\langle i^{(0)}|\hat{\boldsymbol{V}}|i^{(0)}\rangle - \langle 0|\hat{\boldsymbol{V}}|0\rangle][\langle i^{(0)}|\hat{\boldsymbol{Q}}_{\boldsymbol{dyn}}|i^{(0)}\rangle - \langle 0|\hat{\boldsymbol{Q}}_{\boldsymbol{dyn}}|0\rangle] = \omega_{0i}^{0} + R_{dyn}^{SS}(P_{0i}^{\Delta}) \tag{2}$$

In eqs 1 and 2, $\hat{\boldsymbol{V}}$ corresponds to the molecular electrostatic potential operator, while $\hat{\boldsymbol{Q}}_{\boldsymbol{dyn}}$ corresponds to the dynamical apparent charge operator. $|i^{(0)}\rangle$ is the $i$th electronic state obtained in the presence of the fixed reaction field due to the ground state $|0\rangle$. We note that eqs 1 and 2 provide an overview of the leading-order terms, but in the actual implementation of the different schemes the LR is always included in the response matrix.

In the LR formulation, the response ($R_{dyn}$) of the solvent dynamic polarization to the excitation is computed from the transition density ($P_{0i}^{T}$) while in the SS approach the same polarization is determined by the difference of the electron densities of the initial and final states ($P_{0i}^{\Delta}$).

We note that the analysis described so far for transition processes from ground to excited states can be reverted, and the same LR and SS approaches can be applied to emission processes: the difference is that this time the initial equilibrium refers to the excited state while the nonequilibrium description is applied to the vertical ground state.

The LR formulation is the most widely used in combination with TD-DFT as the transition density from ground to excited state is a quantity directly available with TD-DFT, but it accounts for a correction which, based on a comparison with the semiclassical derivation of McRae[34] and Liptay,[35] can be classified as a part of a dispersion-like term[25,26] or as an excitonic coupling term to the solvent molecules, due to the transition density of the solute and the dynamic response of the reaction field.[14] By contrast, the SS scheme, requiring that the change of electron density due to the excitation is known, is naturally coupled with state-specific wave function formulations such as configuration interaction (CI) or complete active space (CAS) approaches, and accounts for the electrostatic equilibration of the solvent to the excited state density. In fact, the latter can be obtained also from TD-DFT thanks to its extension to analytical gradients.[36−39] This opened the way to two SS reformulations of TD-DFT with PCM: the corrected-LR[27] (cLR) and the vertical excitation method[28] (VEM). In both approaches the excitation energy is calculated in a SS fashion (as in eq 2), but within VEM an iterative scheme is used in which the solvent contribution is self-consistently obtained with $P_{0i}^{\Delta}$ while the cLR approach can be seen as the first cycle of this iterative process. An alternative SS approach has been proposed by Improta, Barone, Scalmani, and Frisch[29] (IBSF): it also uses an iterative scheme, but the iterations are performed on the total excited state density ($P_i = P_0 + P_{0i}^{\Delta}$) and therefore the ground state contribution is also recalculated by iterating the KS-DFT equation in the presence of solvent charges calculated for the excited state.

The LR formulation is generally well-suited for transitions which are characterized by a small change of the electron density, because the electrostatic interaction between the solvent and the excited state density is not very different from that of the ground state.[11,13,27,28] By contrast, for excitations involving a large density rearrangement the LR scheme is insufficient because the density-dependent relaxation of the solvent polarization is not included. In those cases, the difference between LR and SS schemes can therefore become significant.[13,26,28,40] These are the cases here investigated, considering two systems: a quadrupolar BODIPY fluorophore and the Nile Red molecule.

## 3. COMPUTATIONAL DETAILS

All DFT and TD-DFT calculations have been carried out with a locally modified version of the Gaussian 09 program,[41] using several global hybrids (GHs) xc-functionals and one range-separated hybrid (RSH) functional. More specifically, for the BODIPY derivative, ground state geometry optimizations, and absorption simulations in dichloromethane have been carried out by exploring the range from 0 to 90% of exact exchange (EEX) coupled to the generalized gradient approximation (GGA) functional PBE.[42] The employed atomic basis set is 6-31G(d). Concerning the Nile Red, ground and excited state structures together with vertical excitation processes in *n*-hexane and acetonitrile have been determined using the B3LYP,[43] PBE0-1/3[44] and CAM-B3LYP[45] xc-functionals. The employed atomic basis set is 6-311G(d,p). To ascertain the convergence of the transition energies, we carried out some tests with the 6-31+G(d,p) in a precedent work:[46] differences smaller than 0.04 eV were found for the first transition in *n*-heptane and vacuo. Solvent effects have been introduced by


DOI: 10.1021/acs.jctc.5b00679
J. Chem. Theory Comput. 2015, 11, 5782−5790

exploiting the IEF-PCM[47] approach with a molecule-shaped cavity made of interlocking spheres centered on heavy atoms. The model set of sphere radii UFF, which is the default in the Gaussian 09 code, has been employed in the case of the BODIPY derivative. The model set of sphere radii UA0, that was the default in the Gaussian 03 code, has been used for NR in order to allow direct comparisons with our precedent investigation on the dual fluorescence of this system in apolar solvent.[46] We have also checked that our general results and conclusions do not change as a function of the model set used. The VEM calculations have been carried out in the diagonal version of the method considering the total relaxed density (RD) (see ref 28 for details).

## 4. RESULTS

To investigate the importance of a proper combination of the polarization model and the xc-functional in cases of large density rearrangements upon excitation, we have selected two prototypical cases of charge-transfer excitations, namely, the absorption of a substituted boron-dipyrromethene (4,4-difluoro-4-bora-3*a*,4*a*-diaza-*s*-indacene, BODIPY), and the Nile Red emission (diethylamino-5*H*-benzo[*a*]phenoxazin-5-one, NR). The structures of both chromophores are reported in Figure 1.

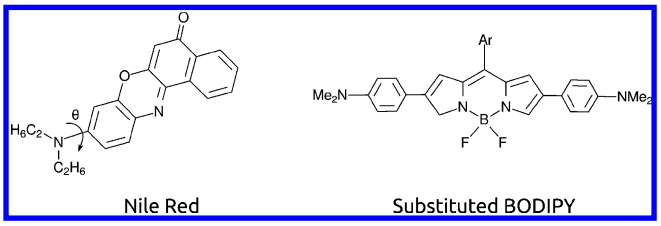


**Figure 1.** Structures of the studied systems: Nile Red (diethylamino-5*H*-benzo[*a*]phenoxazin-5-one, left) and the substituted BODIPY (boron-dipyrromethene, right). In the latter Ar stands for the mesityl ring. The investigated dihedral angle ($\theta$) of Nile Red is also indicated.

**4.1. CT Transition in a Quadrupolar System: The BODIPY Case.** In this section we investigate the influence of EEX percentage on different polarization schemes in the simulation of the BODIPY that undergoes a bright $\pi-\pi^*$ excitation, which can be mainly described as a CT transition from HOMO to LUMO, mainly of quadrupolar character: the dipole moment is not null; nevertheless, the ground to excited state dipole variation is small. The HOMO is principally described as a mixing of a *n*-type orbital of the dimethylamino group and a $\pi$-type orbital due to the pyrrolic moieties. With the increasing of EEX percentage, the $\pi$ character of the HOMO increases, even if the overall shape is maintained (see Figure S1 in the Supporting Information). In Table 1, we collect the results obtained applying the LR and the three SS approaches.

The information available from the experiment is a broad absorption band at 686 nm (1.81 eV) in $CH_2Cl_2$, whereas the emission is completely quenched.[48] To provide a detailed analysis, it is useful to reintroduce the previously presented two-step process (see above) and focus on the polarization response defined with respect to the excitation energy ($\omega_0$) obtained within a frozen ground state polarization (see eqs 1 and 2). These data are reported in Figure 2 for the different LR and SS approaches. In the case of the IBSF scheme, we have used the same $\omega_0$ value that is common to all other schemes as this method does not explicitly calculate this quantity (see Table 1).

**Table 1. Non-Equilibrium Absorption Energies (eV) of the Substituted BODIPY in $CH_2Cl_2$, Using PBE Based GHs Functionals**

| EEX % | $\omega_0$ | LR | cLR | VEM-RD | IBSF |
|---|---|---|---|---|---|
| 0 | 1.23 | 1.19 | 1.20 | 1.04 | 0.96 |
| 10 | 1.49 | 1.44 | 1.40 | 1.27 | 1.10 |
| 20 | 1.75 | 1.71 | 1.66 | 1.54 | 1.29 |
| 25 | 1.89 | 1.84 | 1.79 | 1.68 | 1.42 |
| 30 | 2.02 | 1.97 | 1.93 | 1.82 | 1.56 |
| 40 | 2.27 | 2.20 | 2.20 | 2.09 | 1.99 |
| 50 | 2.48 | 2.40 | 2.43 | 2.33 | 2.28 |
| 60 | 2.65 | 2.56 | 2.62 | 2.53 | 2.52 |
| 70 | 2.79 | 2.68 | 2.77 | 2.69 | 2.72 |
| 80 | 2.89 | 2.77 | 2.88 | 2.82 | 2.85 |
| 90 | 2.97 | 2.84 | 2.96 | 2.91 | 2.96 |

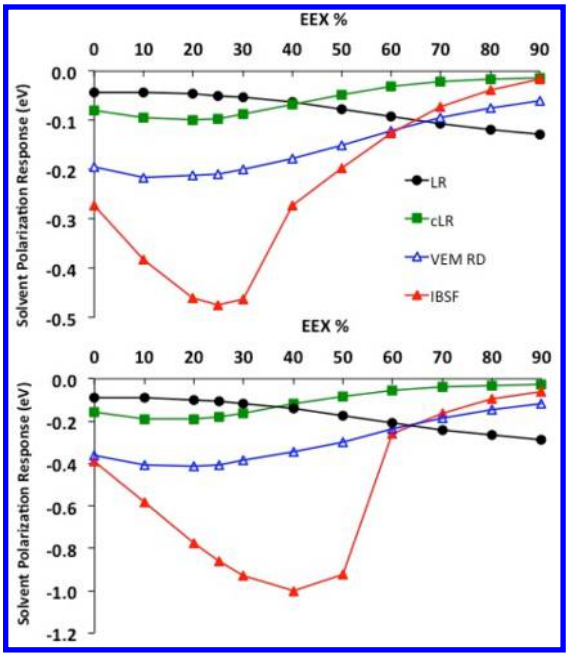


**Figure 2.** Nonequilibrium (up) and equilibrium (down) solvent polarization response (eV) for the first excited singlet state of substituted BODIPY compound, in function of EEX percentage coupled to the PBE parent functional.

The results reported in Figure 2 clearly show that LR has an opposite behavior with respect to all the SS schemes. In the LR case, the absolute value of the solvent polarization term increases when increasing the exact exchange included in the functional, first smoothly and slowly in the range 0−30% of EEX and then more sharply from 30% to 90%. The curvature of all the SS descriptions is instead qualitatively opposite: the absolute value of the solvent polarization term increases only in the range going from 0 to 20−25% of EEX, and then it decreases. Comparing the different SS schemes, one notes that the effect of self-consistency introduced in VEM-RD allows a more complete description of the excited state polarization energy with respect to cLR. On the other hand, as cLR can be considered the first iteration of VEM-RD, it is not surprising that they display similar curvatures. Moreover, the larger effects introduced through the modified ground-state molecular orbitals and orbital energies during the iterations in the IBSF


DOI: 10.1021/acs.jctc.5b00679
J. Chem. Theory Comput. 2015, 11, 5782−5790

scheme are well highlighted in Figure 2. For example, around the typical values of the most widely used GH functionals, such as PBE0, the IBSF correction is around 0.4 eV, a value unexpectedly large for a quadrupolar system. These effects become dramatically large if a complete equilibrium solvation is allowed (Figure 2, at the bottom), and a collapse into the ground state becomes possible. In addition, we note that, only with a large amount of EEX (more than 50%), the IBSF values become of the same order of the other schemes, actually almost interpolating between VEM-RD and cLR schemes. Note that for other BODIPY-like dyes presenting a dipolar rather than a quadrupolar nature, such inadequacy of the IBSF scheme when combined with low EEX functionals has already been reported.[49,50]

The observed behaviors can be rationalized by using a very simplified quantum mechanical model, to obtain more transparent equations: we extend here the model of ref 25 designed for a dipole in a spherical cavity to a quadrupole which better fits the nature of the BODIPY. It is necessary to find the reaction field induced by the quadrupolar moment of the solute molecule inside a spherical cavity of radius $R$. The quadrupolar moment is a rank-two traceless tensor of component:

$$\Theta_{\alpha\beta} = \frac{1}{2}\int \rho(3\boldsymbol{r}_{\alpha}\cdot\boldsymbol{r}_{\beta} - r^2\delta_{\alpha\beta})\,\mathrm{d}\boldsymbol{r} \tag{3}$$

The amplitude of $\boldsymbol{\Theta}$ depends on the choice of the coordinate's origin (unless the dipole moment is null), but if one of the axes (let say $x$-axis for instance) is taken along the axis of the quadrupole moment, the nonzero components are related as follows: $\bar{\Theta} = \Theta_{xx} = -2\Theta_{yy} = -2\Theta_{zz}$. This quantity is often used as the scalar quadrupole strength of the quadrupolar moment tensor. The reaction field for an axial quadrupolar moment in a spherical cavity is[51]:

$$Q(\varepsilon, R) = \mathrm{g}(\varepsilon, R)\bar{\Theta} = \frac{3(\varepsilon - 1)}{3\varepsilon + 2}\frac{1}{R^5}\bar{\Theta} \tag{4}$$

and the quadrupolar term of the solute−solvent interaction potential becomes:

$$\hat{V}(\Psi) = -\hat{\bar{\Theta}}\cdot\mathrm{g}(\varepsilon, R)\left\langle\Psi|\hat{\bar{\Theta}}|\Psi\right\rangle \tag{5}$$

It is easy to recognize that the form of this equation is equivalent to defining the operators $\hat{\boldsymbol{V}}$ and $\hat{\boldsymbol{Q}}_{dyn}$ of eqs 1 and 2, as $\hat{\bar{\Theta}}$ and $-\mathrm{g}_{dyn}(\varepsilon_\infty, R)\hat{\bar{\Theta}}$, respectively.

The pure quadrupolar term of the solvent polarization response in this simplified approach is then

$$\begin{aligned} R_{dyn}^{LR,Q} &= \langle i^{(0)}|\bar{\Theta}|0\rangle\langle 0|-\mathrm{g}_{dyn}(\varepsilon_\infty, R)\bar{\Theta}|i^{(0)}\rangle \\ &= -\mathrm{g}_{dyn}(\varepsilon_\infty, R)\|\bar{\Theta}_{i0}\|^2 \end{aligned} \tag{6}$$

$$\begin{aligned} R_{dyn}^{SS,Q} &= \frac{1}{2}[\langle i^{(0)}|\bar{\Theta}|i^{(0)}\rangle - \langle 0|\bar{\Theta}|0\rangle] \\ &\quad [\langle i^{(0)}|-\mathrm{g}_{dyn}(\varepsilon_\infty, R)\bar{\Theta}|i^{(0)}\rangle + \langle 0|\mathrm{g}_{dyn}(\varepsilon_\infty, R)\bar{\Theta}|0\rangle] \\ &= -\frac{1}{2}\mathrm{g}_{dyn}(\varepsilon_\infty, R)(\bar{\Theta}_{ii} - \bar{\Theta}_{00})^2 \end{aligned} \tag{7}$$

in the LR and SS approach, respectively. Discarding all dipole−quadrupole crossed terms, the total response can be approximated as

$$R_{dyn}^{LR} \approx -f_{dyn}(\varepsilon_\infty, R)\|\boldsymbol{\mu}_{i0}\|^2 - \mathrm{g}_{dyn}(\varepsilon_\infty, R)\|\bar{\Theta}_{i0}\|^2 \tag{8}$$

$$R_{dyn}^{SS} \approx -\frac{1}{2}f_{dyn}(\varepsilon_\infty, R)(\mu_{ii} - \mu_{00})^2 - \frac{1}{2}\mathrm{g}_{dyn}(\varepsilon_\infty, R)(\bar{\Theta}_{ii} - \bar{\Theta}_{00})^2 \tag{9}$$

where $f_{dyn}$ and $\mathrm{g}_{dyn}$ are the reaction field factors for a dipole and a quadrupole in a spherical cavity, respectively.

In Figure 3, dipolar and quadrupolar properties of BODIPY are reported. We note the correlation of the shape of the LR

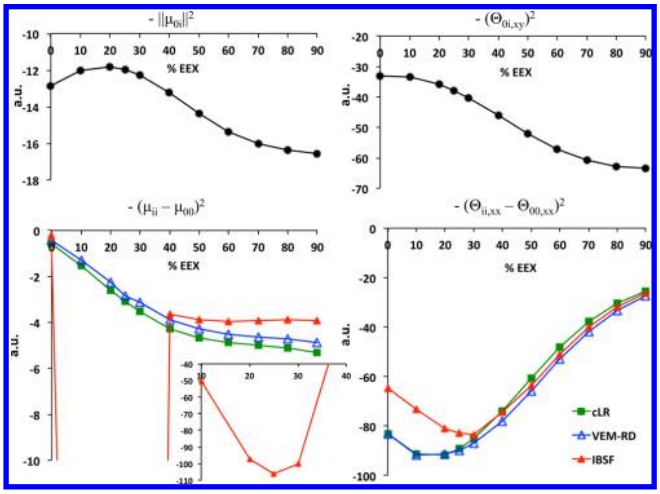


**Figure 3.** Transition (up) and ground-to-excited variation (down) of multipolar moments (a.u.) for the first excited singlet state of substituted BODIPY compound, in function of EEX percentage coupled to the PBE parent functional. Color code: black, LR; green, cLR; blue, VEM-RD; red, IBSF.

solvent polarization response curve (Figure 2) with both the behavior of the transition dipole and the leading term of the transition quadrupole (along the $xy$ axis). On the other hand, the shapes of cLR and VEM solvent polarization responses are in agreement with the leading quadrupolar term $-(\bar{\Theta}_{ii} - \bar{\Theta}_{00})^2$, due to the small ground to excited state dipole variation. The origin of the anomalous behavior for the IBSF polarization is evident in the inset of Figure 3: the effects introduced through the modified ground-state molecular orbitals during the iterations cause an overestimation of the dipolar term (the excited state becomes largely dipolar) as well as a small underestimation of the quadrupolar one in the range 10−30% of EEX included in the functional used. This different "dipolar" behavior of IBSF is related to the nonvariational character of the GS energy part: as the excited state dipole is the sum of GS and response to the perturbation, the nonvariational character of the GS energy part of the IBSF scheme[52]—even for relatively small changes (see Figure S2 in the Supporting Information)—can induce large variations of the corresponding dipole because the dipole is related to the field-derivative of the energy.

**4.2. Nile Red Relaxed Potential Energy Surfaces in Polar and Apolar Solvents.** NR presents a fluorescence spectrum with two peaks centered at ca. 530 and ca. 570 nm in apolar solvents.[53,54] Though modulated, this behavior is retained in many nonprotic media[55] and also in more complex chemical environments such as binary solvent mixtures with a high water ratio[53] or reverse micelles.[54] However, this is not the case in isotropic solutions with increasing solvent polarity,[56]


DOI: 10.1021/acs.jctc.5b00679
J. Chem. Theory Comput. 2015, 11, 5782−5790

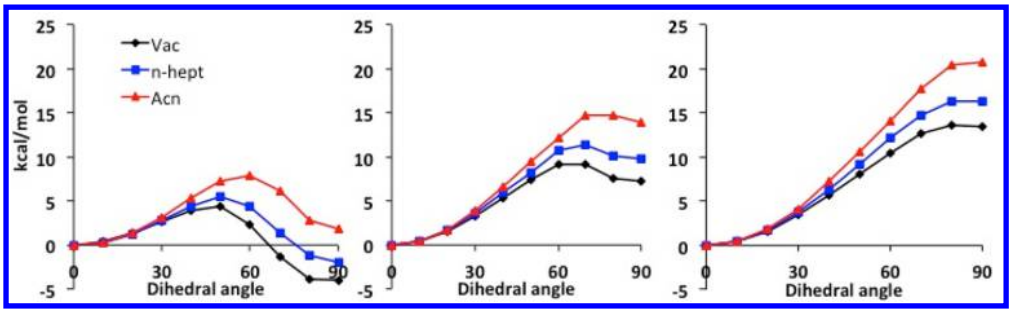


**Figure 4.** LR-PCM relative relaxed PESs (in kcal/mol) of NR at the first singlet excited state, calculated in different environments (gas phase, black; *n*-heptane, blue; acetonitrile, red), as a function of the dihedral angle between dimethylamino group and the molecular plane. Left: B3LYP; middle: PBE0-1/3; right: CAM-B3LYP.

e.g., acetonitrile,[57] where no band splitting is detected for absorption nor emission, whereas in water the emission is completely quenched. In the past, the experimental studies[53,56,58,59] suggested that the peculiar spectroscopic fingerprint in apolar solvent could be related to a twisted intramolecular charge transfer (TICT) process, the same mechanism used to explain the anomalous dual fluorescence of 4,4′-dimethylaminobenzonitrile (DMABN).[60] However, few years ago, using the CAM-B3LYP xc-functional and the cLR polarization scheme, we showed[46] that the dual fluorescence of Nile Red in *n*-heptane is in fact the result of a strongly active vibronic coupling, thus supporting a planar rather than a twisted ICT in that medium.

Here, we extended the analysis to the impact of the interplay between the selected xc-functional and the polarization scheme used for the description of the relaxed potential energy surface (PES) and notably the twisting of dimethylamino group considered in both apolar (*n*-heptane) and polar (acetonitrile) solvents. From a physical point of view, due to the very large dipole moment, increasing the solvent polarity should stabilize the formation of the TICT state and concomitantly decrease the torsional barrier of the excited state PES. Experimentally the double-peak structure of the emission is blue-shifted to a single peak when going from *n*-heptane[55] to acetonitrile,[58] while the quantum yield (0.76) and fluorescence lifetime (4.7 ns) remain large.[61] From these observations one can conclude that, even if a second minimum could be found in the PES corresponding to a twisted structure in acetonitrile, the torsional barrier should still be sufficiently high to prevent the (bright) planar conformation to reach the dark TICT state. In water instead, we expect that the barrier becomes negligible as the emission is quenched:[55,61] this can be related to the combination of the polarity and the hydrogen bond effects which both largely stabilize the TICT structure.

The TD-DFT/PCM description of the involved PES is largely dependent on both the functional and the polarization scheme as shown in Figure 4 where we compare the excited state energy with respect to the torsional angle as obtained within the LR description using three different functionals.

The comparison of the three different functionals (B3LYP, PBE0-1/3, and CAM-B3LYP) shows that a very stable twisted minimum is found with B3LYP optimizations, both in acetonitrile and *n*-heptane, as well as in gas phase. Even if this picture seems to be coherent with expectations (at least in acetonitrile), it instead comes from an error cancellation process, as demonstrated in the following. Indeed, it is important to note that moving from an apolar (*n*-heptane) to a polar (acetonitrile) solvent, the LR scheme with all functionals predicts both an increase of the torsional barrier (see Table 2) and a decrease of the relative stability of the $S_1$ state at the twisted structure, these two outcomes going against the expected physical trend.

**Table 2. Height of Torsional Barriers (kcal/mol) of NR in Different Solvents for the Different Schemes of Polarization**

| scheme | solvent | B3LYP | PBE0-1/3 | CAM-B3LYP |
|---|---|---|---|---|
| LR | *n*-heptane | 5.5 | 11.3 | 16.3 |
| | acetonitrile | 7.9 | 14.8 | 20.7 |
| cLR | *n*-heptane | 3.6 | 8.6 | 15.4 |
| | acetonitrile | 3.3 | 7.5 | 15.0 |
| VEM-RD | *n*-heptane | 2.8 | 7.2 | 13.6 |
| | acetonitrile | 1.6 | 5.2 | 10.3 |
| IBSF | *n*-heptane | 2.3 | 6.2 | 15.7 |
| | acetonitrile | 1.7 | 4.8 | 9.1 |

The observed differences in the description of the process for the different functionals are evidenced in Figure 5, where the PES of the first and second singlet excited states are reported, together with the variation of the oscillator strengths during the twisting in acetonitrile (the same behavior is qualitatively obtained both in vacuo and *n*-heptane, data not shown).

The presence of a second minimum in both B3LYP and PBE0-1/3 PESs is a consequence of the variation of the nature of $S_1$ state PES from a bright to a dark state and vice versa for $S_2$ along the dihedral torsion. Increasing the EEX percentage included in the xc-functional, the overstabilization of the dark state at the twisted structure is largely reduced with PBE0-1/3 (33% of EEX). By contrast, CAM-B3LYP (EEX modulated from 19% to 65% depending on the interelectronic distance) provides PESs that do not change from a bright to a dark state along the dihedral torsion, and the second minimum is observed for $S_2$. B3LYP and PBE0-1/3 behaviors are a consequence of the well-known CT overstabilization of low EEX percentage GH functionals. This overstabilization compensates the erroneous polarization scheme in LR-PCM, which does not include the explicit relaxation of the solvent polarization with respect to the excited state density.

The CT nature of the states has been investigated by estimating the associated effective electronic displacement during the excitation, by the recently proposed metric Γ,[62] particularly in its natural transition orbital[63] (NTO) based version, $\Gamma_{NTO}$. Indeed, this procedure allows identifying the "principal components" of the transition electron density (by using NTO) and provides a measure of the interaction distance between the hole and the particle. As shown in Figure 6, for the



DOI: 10.1021/acs.jctc.5b00679
J. Chem. Theory Comput. 2015, 11, 5782−5790

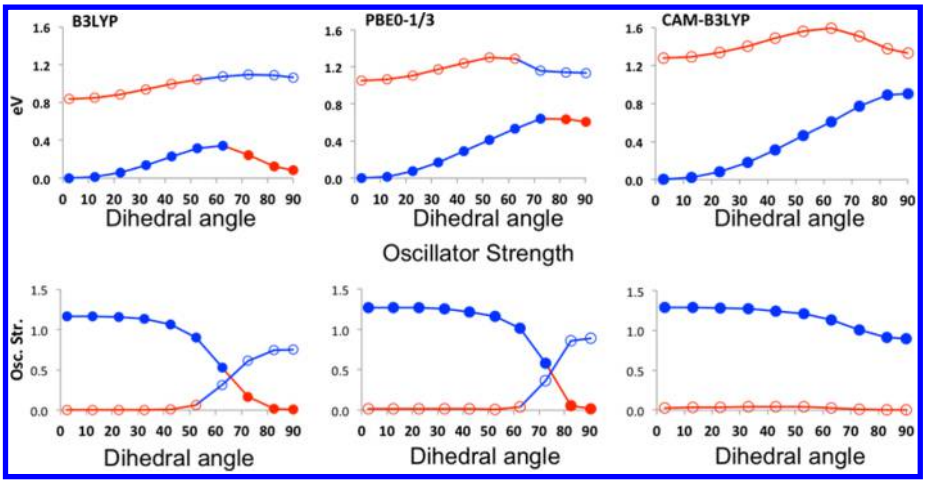


**Figure 5.** $S_1$ (closed points) and $S_2$ (open points) LR-PCM relative relaxed PESs (in eV) of Nile Red calculated in acetonitrile with B3LYP, PBE0-1/3, and CAM-B3LYP functionals, and relative oscillator strength (red, dark excitations; blue, bright excitations).

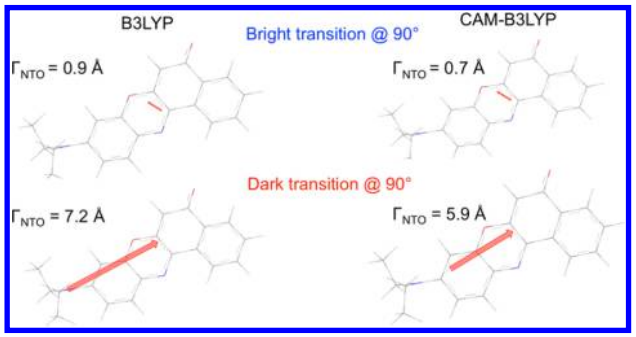


**Figure 6.** Nile Red interaction distance of the hole−particle pairs measured by the $\Gamma_{NTO}$ metric (in Å) in acetonitrile at the optimized twisted (90°) structures for the bright (up) and dark (down) transitions.

twisted structures determined by LR-PCM, the dark transition shows a very large electron displacement. We underline that the CT character of the dark transition obtained from B3LYP calculation is stronger than at the CAM-B3LYP level.

Figure 7 shows that by introducing SS-type corrections, a second minimum can be individuated in the PES of NR in acetonitrile for all functionals, including CAM-B3LYP. Most important, the dark excited state at the twisted structure becomes more stable by increasing the solvent polarity, and in parallel the torsional barrier is reduced, as reported in Table 2. We note that, due to the fact that the SS corrections are single point calculations on LR structures, it is important that when an SS model is applied the geometry used should be consistent with the nature of the state investigated. For example, in the case of CAM-B3LYP in acetonitrile, the SS energy values corresponding to the lowest excited state at 80° and 90° of twisting have been obtained using the geometry of the $S_2$ state of the LR model as this is the CT state. If one would have used the $S_1$ LR structure, the SS stabilization would have been less (as referring to the valence bright state). In general, studying the TICT processes, it is a good strategy to optimize the geometry for both states and then to do SS calculation for both states on both structures. For instance, this same procedure was

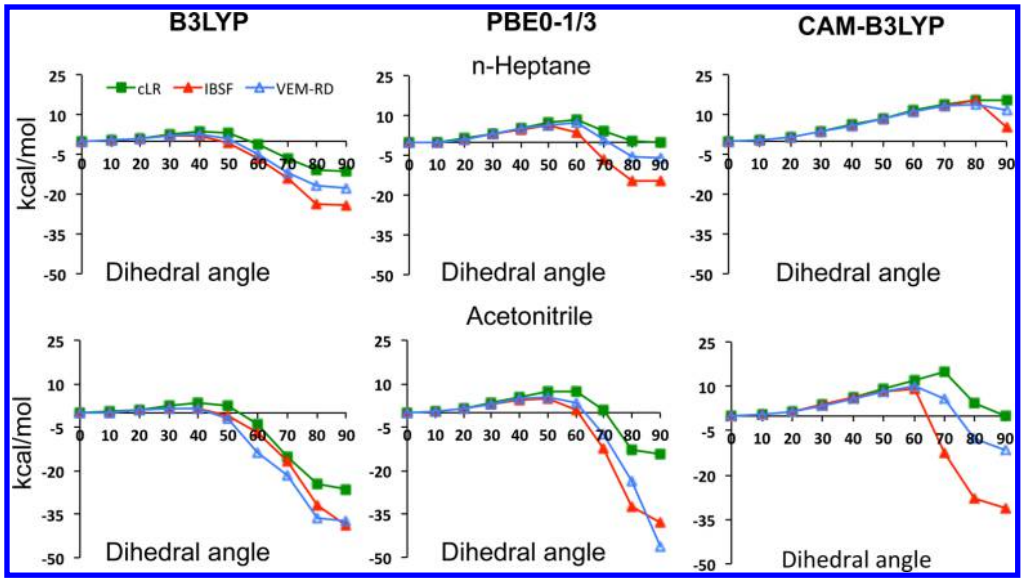


**Figure 7.** SS relaxed PESs (in kcal/mol) of Nile Red first excited state, calculated in different solvents (*n*-heptane, top; acetonitrile, bottom) with B3LYP (left), PBE0-1/3 (middle), and CAM-B3LYP (right). All values are referred to that of the planar structure.



DOI: 10.1021/acs.jctc.5b00679
J. Chem. Theory Comput. 2015, 11, 5782−5790

also applied in the apolar solvent case, but the inversion was not found.

The introduction of the SS corrections also highlights the large discrepancies among the different functionals. GH functionals (B3LYP and PBE0-1/3) yield similar trends in both solvents, with lower barriers and more stabilized twisted structures than CAM-B3LYP. The overstabilization of CT states for GH functionals with low EEX percentage causes an underestimation of barriers in both solvents, which is particularly large in the B3LYP case: for VEM-RD and IBSF, the barrier in acetonitrile is ca. 1.8 kcal/mol, while it increases to ca. 3 kcal/mol by using cLR. From these data one can conclude that B3LYP calculations incorrectly predict that the NR in acetonitrile is prone to overcome the torsional barrier around the dimethyl amino group in its first excited state, quenching the emission. The B3LYP behavior obtained here is in line with the analysis of TD-DFT performances performed in gas-phase for TICT processes in both DMABN[64] and a fluorescent yellow pigment.[65]

The use of RSH xc-functional largely changes the landscape: SS CAM-B3LYP calculations yield a clearly TICT stable state only in acetonitrile for all the solvent schemes used, whereas a second minimum, but less stable than the planar one, is found with VEM-RD and IBSF schemes in *n*-heptane. This confirms the PICT picture we obtained in our precedent work based on cLR,[27] considering that all SS approaches predict torsional barriers larger than 13 kcal/mol in *n*-heptane. More importantly, the SS CAM-B3LYP barriers in both solvents are larger than 9 kcal/mol (see Table 2), and therefore the emissive state is predicted to present a planar conformation.

As a further comment, we note that the IBSF approach can give rise to a large overstabilization effect of the TICT state in the polar solvent even in the case of RSH functionals, and therefore care should be paid in using this method for such a kind of states. This specificity of the method could probably have played a role in the results reported by Pedone in studying the TICT process in a 7-aminocoumarin system,[32] where CAM-B3LYP/IBSF calculations suggested the formation of a TICT state and an intersection between the ground and first excited singlet adiabatic PESs.

As a further analysis, it is interesting to quantify the effects of the functional on the geometry. In Figure 8 we compare B3LYP LR and SS single point calculations on both CAM-B3LYP and B3LYP structures.

As it can be seen in Figure 8, the B3LYP PESs for the different polarization schemes are very similar for both structures. Therefore, the B3LYP and CAM-B3LYP structures used for the SS PESs are analogues, and choosing one or the other does not affect the main conclusions. However, based on previous studies of excited state structure optimizations in both gas phase and solution,[66−68] we expect that the most appropriate structures for medium or large chromophores are that obtained by using the CAM-B3LYP (particularly for excitations involving large reorganization of density upon excitation, such as for push−pull chromophores[66]).

To complete our analysis, we have investigated the accuracy of the different functionals when combined with the different polarization schemes in reproducing the experimental Stokes shift. The data are reported in Table 3. According to Figures 5 and 7 and Table 2, all the emission values have been calculated from the planar minima except in the case of SS polarization schemes coupled to B3LYP functional for which the structure of the 60° minimum has been used. From the data reported in

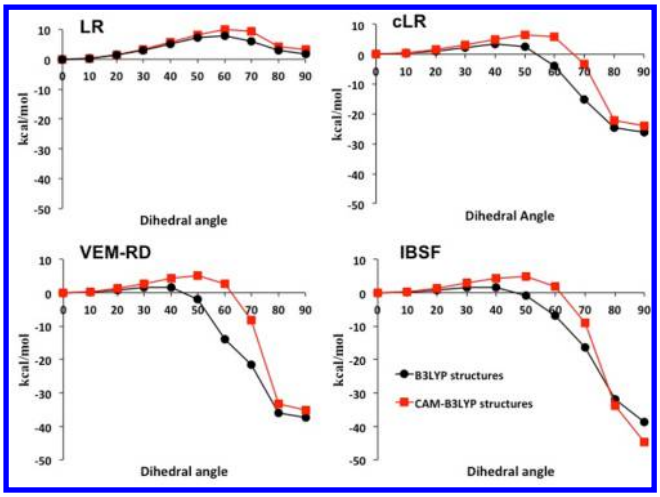


**Figure 8.** B3LYP single point relative energies (in kcal/mol) of NR first excited state, calculated using the different polarization schemes for structures determined by LR/B3LYP (black) and LR/CAM-B3LYP (red) optimizations. All values are referred to that of the corresponding planar structure.

Table 3, it comes out that a good reproduction of the experimental data can be obtained either by combining B3LYP with LR or CAM-B3LYP with SS approaches. In particular, in these two cases the energy overestimation with respect to the experimental data is of the same quantity for both absorption and emission, resulting in a good reproduction of the experimental Stokes shift. However, the good behavior of B3LYP-LR is only valid in the "local" (i.e., single point) description of the PES, which is generally not physically correct.

## 5. CONCLUSIONS

In this study we have critically analyzed and compared different polarization schemes derived from LR and SS formulations of the TD-DFT/PCM strategy and their coupling with different xc-functionals. The key role of the selected SS scheme and its strong interplay with the chosen functional have been pointed out, by testing two prototypical cases of charge-transfer excitations, namely, the absorption of a substituted BODIPY and the excited state geometrical relaxation and the following emission of Nile Red.

The risk of overpolarization effects due to a nonoptimal selection of xc-functional in cases of large density rearrangements upon excitation has been illustrated: the type of functional used determines the strength of the polarization by the predicted transition dipoles as well as the ground to excited state dipole (or quadrupole) variations. Even in the case of a state specific approach, the overestimation of these molecular properties can lead to a wrong description of the solvent polarization response.

Our results point out that, for CT-like transitions of molecules in solution, the description obtained from GH functionals (such as B3LYP or PBE0-1/3) coupled to a LR scheme can yield to results which apparently provide numerical values close to experiments, but this apparent match is due to an error compensation: the well-known CT overstabilization of low EEX percentage GH functionals compensates the missed description of polarization effects in LR-PCM for this family of states. When instead, the important explicit contribution due to the relaxation of the solvent polarization in the excited state is


DOI: 10.1021/acs.jctc.5b00679
J. Chem. Theory Comput. 2015, 11, 5782−5790

Table 3. Nile Red Absorption, Emission and Stokes Shift (in eV) in Acetonitrile, Obtained with the Different Polarization Schemes[a]

| functional | LR | cLR | VEM-RD | IBSF | experimental[48,51] |
|---|---|---|---|---|---|
| | | | Absorption | | |
| B3LYP | 2.48 | 2.56 | 2.52 | 2.42 | 2.31 |
| PBE0-1/3 | 2.66 | 2.75 | 2.71 | 2.59 | |
| CAM-B3LYP | 2.82 | 2.90 | 2.84 | 2.71 | |
| | | | Emission | | |
| B3LYP | 2.10 (0) | 1.53 (60) | 1.02 (60) | 1.37 (60) | 2.01 |
| PBE0-1/3 | 2.19 (0) | 2.53 (0) | 2.49 (0) | 2.44 (0) | |
| CAM-B3LYP | 2.17 (0) | 2.52 (0) | 2.50 (0) | 2.44 (0) | |
| | | | Stokes Shift | | |
| B3LYP | 0.38 | 1.03 | 1.50 | 1.05 | 0.30 |
| PBE0-1/3 | 0.47 | 0.23 | 0.22 | 0.16 | |
| CAM-B3LYP | 0.66 | 0.37 | 0.34 | 0.27 | |

[a]The dihedral angle of the minimized structure used for emission is reported in parentheses.

introduced through a SS model, the use of a RSH functionals is needed to reach an accurate description, as expected.

## ■ ASSOCIATED CONTENT

### Supporting Information

The Supporting Information is available free of charge on the ACS Publications website at DOI: 10.1021/acs.jctc.5b00679.

Pictures of the MOs involved in the $\pi-\pi^*$ excitation and the SCF energy difference between the first and the last cycle of iteration for each functional in the IBSF scheme for BODIPY system (PDF)

## ■ AUTHOR INFORMATION


### Corresponding Authors

*(C.A.G.) E-mail: ciro.guido@for.unipi.it.
*(B.M.) E-mail: benedetta.mennucci@unipi.it.


### Notes

The authors declare no competing financial interest.

## ■ ACKNOWLEDGMENTS

C.A.G. and B.M. acknowledge the European Research Council (ERC) for financial support in the framework of the Starting Grant (EnLight-277755). D.J. acknowledges the ERC and the Région des Pays de la Loire for financial support in the framework of a Starting Grant (Marches – 278845) and the LUMOMAT RFI project, respectively. Part of this research used resources of CCIPL (Centre de Calcul Intensif des Pays de Loire), the CINES (Centre Informatique National de l'Enseignement Supérieur), and a local Troy cluster.

## ■ REFERENCES


(1) Lakowicz, J. R. *Principle of Fluorescence Spectroscopy*, 3rd ed.; Springer US: New York, U.S.A., 2006.
(2) Reichardt, C. *Chem. Rev.* **1994**, *94*, 2319–2358.
(3) Kamlet, M. J.; Abboud, J. L. M.; Abraham, M. H.; Taft, R. W. *J. Org. Chem.* **1983**, *48*, 2877–2887.
(4) Buncel, E.; Rajagopal, S. *Acc. Chem. Res.* **1990**, *23*, 226–231.
(5) Reichardt, C. *Solvents and Solvent Effects in Organic Chemistry*, 3rd ed.; Wiley-VCH: Weinheim, Germany, 2003.
(6) Tomasi, J.; Mennucci, B.; Cammi, R. *Chem. Rev.* **2005**, *105*, 2999–3093.
(7) Cramer, C.; Truhlar, D. *Chem. Rev.* **1999**, *99*, 2161–2200.
(8) Klamt, A. *Wiley Interdisciplinary Reviews: Computational Molecular Science* **2011**, *1*, 699–709.
(9) Klamt, A. *J. Phys. Chem.* **1996**, *100*, 3349–3353.
(10) Chipman, D. M. *J. Chem. Phys.* **2009**, *131*, 014103.
(11) Mennucci, B.; Cappelli, C.; Guido, C. A.; Cammi, R.; Tomasi, J. *J. Phys. Chem. A* **2009**, *113*, 3009–3020.
(12) Marenich, A. V.; Cramer, C. J.; Truhlar, D. G. *J. Chem. Theory Comput.* **2010**, *6*, 2829–2844.
(13) Jacquemin, D.; Mennucci, B.; Adamo, C. *Phys. Chem. Chem. Phys.* **2011**, *13*, 16987–16998.
(14) Lunkenheimer, B.; Köhn, A. *J. Chem. Theory Comput.* **2013**, *9*, 977–994.
(15) Mewes, J. M.; You, Z. Q.; Wormit, M.; Kriesche, T.; Herbert, J. M.; Dreuw, A. *J. Phys. Chem. A* **2015**, *119*, 5446–5464.
(16) Mennucci, B. *Int. J. Quantum Chem.* **2015**, *115*, 1202–1208.
(17) Runge, E.; Gross, E. K. U. *Phys. Rev. Lett.* **1984**, *52*, 997–1000.
(18) Casida, M. E. Time-Dependent Density Functional Response Theory for Molecules. In *Recent advances in density functional methods*; Chong, D. P., Ed.; World Scientific: Singapore, 1995; Vol. *1*, pp 155–193.
(19) Adamo, C.; Jacquemin, D. *Chem. Soc. Rev.* **2013**, *42*, 845–856. Laurent, A. D.; Jacquemin, D. *Int. J. Quantum Chem.* **2013**, *113*, 2019–2039.
(20) Ruiz-Lopez, M. F.; Rinaldi, D. *J. Mol. Struct.* **1983**, *93*, 277–281; *Chem. Phys.* **1984**, *86*, 367–373.
(21) Mikkelsen, K. V.; Jorgensen, P.; Jensen, H. J. A. *J. Chem. Phys.* **1994**, *100*, 6597.
(22) Christiansen, O.; Nymand, T. M.; Mikkelsen, K. V. *J. Chem. Phys.* **2000**, *113*, 8101.
(23) Cammi, R.; Mennucci, B. *J. Chem. Phys.* **1999**, *110*, 9877.
(24) Cossi, M.; Barone, V. *J. Chem. Phys.* **2001**, *115*, 4708–4717.
(25) Cammi, R.; Corni, S.; Mennucci, B.; Tomasi, J. *J. Chem. Phys.* **2005**, *122*, 104513.
(26) Corni, S.; Cammi, R.; Mennucci, B.; Tomasi, J. *J. Chem. Phys.* **2005**, *123*, 134512.
(27) Caricato, M.; Mennucci, B.; Tomasi, J.; Ingrosso, F.; Cammi, R.; Corni, S.; Scalmani, G. *J. Chem. Phys.* **2006**, *124*, 124520.
(28) Marenich, A. V.; Cramer, C. J.; Truhlar, D. G.; Guido, C. A.; Mennucci, B.; Scalmani, G.; Frisch, M. J. *Chem. Sci.* **2011**, *2*, 2143–2161.
(29) Improta, R.; Barone, V.; Scalmani, G.; Frisch, M. J. *J. Chem. Phys.* **2006**, *125*, 054103.
(30) Improta, R. *Phys. Chem. Chem. Phys.* **2008**, *10*, 2656–2664.
(31) Pedone, A.; Gambuzzi, E.; Barone, V.; Bonacchi, S.; Genovese, D.; Rampazzo, E.; Prodi, L.; Montalti, M. *Phys. Chem. Chem. Phys.* **2013**, *15*, 12360–12372.
(32) Pedone, A. *J. Chem. Theory Comput.* **2013**, *9*, 4087–4096.
(33) Aguilar, M. *J. Phys. Chem. A* **2001**, *105*, 10393–10396.
(34) McRae, M. G. *J. Phys. Chem.* **1957**, *61*, 562–572.
(35) Liptay, W. In *Modern Quantum Chemistry, Part II*; Sinanoglu, O., Ed.; Academic Press: New York, U.S.A., 1966; Chapter 5.




DOI: 10.1021/acs.jctc.5b00679
*J. Chem. Theory Comput.* 2015, 11, 5782–5790

(36) Van Caillie, C.; Amos, R. D. *Chem. Phys. Lett.* **1999**, *308*, 249−255.
(37) Van Caillie, C.; Amos, R. D. *Chem. Phys. Lett.* **2000**, *317*, 159−164.
(38) Furche, F.; Ahlrichs, R. *J. Chem. Phys.* **2004**, *117*, 7433.
(39) Scalmani, G.; Frisch, M. J.; Mennucci, B.; Tomasi, J.; Cammi, R.; Barone, V. *J. Chem. Phys.* **2006**, *124*, 094107.
(40) Lunkenheimer, B.; Köhn, A. *J. Chem. Theory Comput.* **2013**, *9*, 977−994.
(41) Frisch, M. J.; Trucks, G. W.; Schlegel, H. B.; Scuseria, G. E.; Robb, M. A.; Cheeseman, J. R.; Scalmani, G.; Barone, V.; Mennucci, B.; Petersson, G. A.; Nakatsuji, H.; Caricato, M.; Li, X.; Hratchian, H. P.; Izmaylov, A. F.; Bloino, J.; Zheng, G.; Sonnenberg, J. L.; Hada, M.; Ehara, M.; Toyota, K.; Fukuda, R.; Hasegawa, J.; Ishida, M.; Nakajima, T.; Honda, Y.; Kitao, O.; Nakai, H.; Vreven, T.; Montgomery, J. A., Jr.; Peralta, J. E.; Ogliaro, F.; Bearpark, M.; Heyd, J. J.; Brothers, E.; Kudin, K. N.; Staroverov, V. N.; Kobayashi, R.; Normand, J.; Raghavachari, K.; Rendell, A.; Burant, J. C.; Iyengar, S. S.; Tomasi, J.; Cossi, M.; Rega, N.; Millam, J. M.; Klene, M.; Knox, J. E.; Cross, J. B.; Bakken, V.; Adamo, C.; Jaramillo, J.; Gomperts, R.; Stratmann, R. E.; Yazyev, O.; Austin, A. J.; Cammi, R.; Pomelli, C.; Ochterski, J. W.; Martin, R. L.; Morokuma, K.; Zakrzewski, V. G.; Voth, G. A.; Salvador, P.; Dannenberg, J. J.; Dapprich, S.; Daniels, A. D.; Farkas, Ö.; Foresman, J. B.; Ortiz, J. V.; Cioslowski, J.; Fox, D. J. *Gaussian 09 Development Version*, Revision H.11; Gaussian, Inc.: Wallingford, CT, 2009.
(42) Perdew, J. P.; Burke, K.; Ernzerhof, M. *Phys. Rev. Lett.* **1996**, *77*, 3865−3868.
(43) Stephens, P. J.; Devlin, F. J.; Chabalowski, C. F.; Frisch, M. J. *J. Phys. Chem.* **1994**, *98*, 11623−11627.
(44) Guido, C. A.; Brémond, E.; Adamo, C.; Cortona, P. *J. Chem. Phys.* **2013**, *138*, 021104.
(45) Yanai, T.; Tew, D. P.; Handy, N. C. *Chem. Phys. Lett.* **2004**, *393*, 51−57.
(46) Guido, C. A.; Mennucci, B.; Jacquemin, D.; Adamo, C. *Phys. Chem. Chem. Phys.* **2010**, *12*, 8016−8023.
(47) Mennucci, B.; Cances, E.; Tomasi, J. *J. Phys. Chem. B* **1997**, *101*, 10506−10517.
(48) Hayashi, Y.; Yamaguchi, S.; Cha, W. Y.; Kim, D.; Shinokubo, H. *Org. Lett.* **2011**, *13*, 2992−2995.
(49) Chibani, S.; Charaf-Eddin, A.; Le Guennic, B.; Jacquemin, D. *J. Chem. Theory Comput.* **2013**, *9*, 3127−3135.
(50) Chibani, S.; Charaf-Eddin, A.; Mennucci, B.; Le Guennic, B.; Jacquemin, D. *J. Chem. Theory Comput.* **2014**, *10*, 805−810.
(51) Togashi, D. M.; Costa, S. M. B.; Sobra, A. J. F. N.; Gonsalves, A. M. A. N. *Chem. Phys.* **2004**, *300*, 267−275. Ghoneim, N.; Suppan, P. *Spectrochim. Acta, Part A* **1995**, *51*, 1043.
(52) Bjorgaard, J. A.; Velizhanin, K. A.; Tretiak, S. *J. Chem. Phys.* **2015**, *143*, 054305.
(53) Greenspan, P.; Mayer, E. P.; Fowler, S. D. *J. Cell Biol.* **1985**, *100*, 965−973.
(54) Dutt, G. B.; Doraiswamy, S.; Periasamy, N. *J. Chem. Phys.* **1991**, *94*, 5360.
(55) Datta, A.; Mandal, D.; Pal, S. K.; Bhattacharyya, K. *J. Phys. Chem. B* **1997**, *101*, 10221−10225.
(56) Dutta, A. K.; Kamada, K.; Ohta, K. *J. Photochem. Photobiol., A* **1996**, *93*, 57−64.
(57) Jee, A.; Park, S.; Kwon, P.; Lee, M. *Chem. Phys. Lett.* **2009**, *477*, 112−115.
(58) Kawski, A.; Bojarski, P.; Kuklinski, B. *Chem. Phys. Lett.* **2008**, *463*, 410−412.
(59) Sarkar, N.; Das, K.; Nath, D. N.; Bhattacharyya, K. *Langmuir* **1994**, *10*, 326−329.
(60) Rotkiewicz, K.; Grellmann, K. H.; Grabowski, Z. R. *Chem. Phys. Lett.* **1973**, *19*, 315−318;*erratum*: **1973**, *21*, 212.
(61) Cser, A.; Nagy, K.; Biczók, L. *Chem. Phys. Lett.* **2002**, *360*, 473−478.
(62) Guido, C. A.; Cortona, P.; Adamo, C. *J. Chem. Phys.* **2014**, *140*, 104101. Guido, C. A.; Cortona, P.; Adamo, C.; Mennucci, B. *J. Chem. Theory Comput.* **2013**, *9*, 3118−3126.
(63) Martin, R. L. *J. Chem. Phys.* **2003**, *118*, 4775.
(64) Wiggins, P.; Williams, J. A. G.; Tozer, D. J. *J. Chem. Phys.* **2009**, *131*, 091101.
(65) Plötner, J.; Dreuw, A. *Chem. Phys.* **2008**, *347*, 472−482.
(66) Guido, C. A.; Knecht, S.; Kongsted, J.; Mennucci, B. *J. Chem. Theory Comput.* **2013**, *9*, 2209−2220.
(67) Guido, C. A.; Jacquemin, D.; Adamo, C.; Mennucci, B. *J. Phys. Chem. A* **2010**, *114*, 13402−13410.
(68) Bousquet, D.; Fukuda, R.; Maitarad, P.; Jacquemin, D.; Ciofini, I.; Adamo, C.; Ehara, M. *J. Chem. Theory Comput.* **2013**, *9*, 2368−2379.


DOI: 10.1021/acs.jctc.5b00679
*J. Chem. Theory Comput.* 2015, 11, 5782−5790